VNU Journal of Science: Mathematics - Physics

Journal homepage: https://js.vnu.edu.vn/MaP

Original Article

A Proof-of-concept Study on Enhancing the Visible Photoresponse of RGO/ZnO Devices with PbS Quantum Dots

Le Gia Vy[1,2], Le Nhat Quang Khoi[1,2], Luu Kien Quoc[1,2], Vo Van Anh Tai[1,2], Tran Cong Khanh[1,2], La Phan Phuong Ha[1,2], Huynh Tran My Hoa[3], Tran Thuan Phat[1,2], Le Thai Duy[1,2], Dang Vinh Quang[1,2,*]

[1]*University of Science, 227 Nguyen Van Cu, Cho Quan, Ho Chi Minh, Vietnam*

[2]*Vietnam National University, Linh Xuan, Ho Chi Minh City, Vietnam*

[3]*Nguyen Tat Thanh University, 298-300A Nguyen Tat Thanh, Xom Chieu, Ho Chi Minh, Vietnam*

Received 26th August 2025
Revised 25th October 2025; Accepted 02nd March 2026

Abstract: Hybrid structures of zinc oxide nanorods (ZnO NRs) and reduced graphene oxide (RGO) are a promising platform for photodetection applications, owing to their excellent charge transport pathways and high stability. However, their operational range is intrinsically limited to the ultraviolet (UV) spectrum due to the wide optical band gap of ZnO (~3.37 eV), restricting their applicability in broadband photodetection. To circumvent this issue, in this study, we introduce lead sulfide quantum dots (PbS QDs) decoration to the RGO/ZnO-based photodetector. The deposition of 2 mg mL^{-1} PbS QDs successfully broadened the light absorption capabilities, as evidenced by a decreased optical band gap from 3.19 to 3.13 eV. Consequently, the fabricated RGO/ZnO-PbS NRs heterostructure photodetector demonstrates a remarkable improvement in performance achieving a maximum photocurrent of 292.06 µA, with a 19.5-fold increase in responsivity and photoconductive gain, and nearly three times higher in detectivity, when excited with 395 nm (800 µW) light source. Nonetheless, the device also maintains a repeatable signal pattern over several on/off cycles. Therefore, this work not only presents a highly effective path for engineering the spectral response of ZnO-based devices but also validates the pivotal role of PbS QDs in creating high-performance, broadband photodetectors for next-generation optoelectronic applications.

Keywords: ZnO nanorods, PbS QDs, heterostructure, visible photodetector, tunable optical bandgap.

* Corresponding author.
E-mail address: vinhquangntmk@gmail.com

https//doi.org/10.25073/2588-1124/vnumap.5067

1. Introduction

Optoelectronic devices, operating on the principle of converting photon signals to electrical signals, are becoming the cornerstone of modern technology. They are the enabling platform for applications ranging from optical fiber communications [1], laser diodes [2], light-emitting diodes (LEDs) [3, 4], to solar cells [5, 6]. Likewise, photodetector (PD), a member of this diverse family of devices, have been extensively studied for their role in converting photons into measurable electrical current [7, 8]. Early works on conventional PDs, which rely on well-known semiconductors such as silicon or II–VI compounds (i.e. ZnS, CdSe, etc.), are often fall short in responsivity, response speed, and functional versatility [9]. Therefore, a growing interest has been driven towards hybrid architectures: By combining materials with complementary properties, these hybrids can overcome the limitations of single-component systems and further make ways for enhanced optoelectronic performance.

Among the various reported hybrid systems, ZnO nanostructures integrated with reduced graphene oxide (RGO) has drawn significant attention, owing to its diverse applications [10-12]. Specifically, RGO offers high electrical conductivity, favorable carrier pathways, and chemical stability, while ZnO provides strong optical absorption and versatile morphology control via a variety of synthesis methods. To further leverage these properties, research over the past decade has focused on one-dimensional (1D) ZnO nanostructures, such as nanorods (NRs), which not only maximize the surface-to-volume ratio but also provide direct pathways for efficient charge transport [13].

Despite these widely well-known advantages, photodetectors based on ZnO NRs suffer from one critical limitation: negligible absorption in the visible spectrum, which hinders broader real-world applicability [14-16]. Current research has come up with several solutions to circumvent this issue by creating hybrid structures, aimed to extend the spectral absorption into the visible or infrared regions [17, 18]. To this end, several material modification strategies have been explored. One of which is bandgap tuning through transition metal doping or the decoration of noble metal nanoparticles (e.g., Au, Ag) via utilizing their localized surface plasmon resonance (SPR) effect to boost visible light absorption [19, 20]. However, these methods often suffer from poor reproducibility due to uncontrollable substitution effects in doped systems, or from high material costs in the case of noble metals [21]. These limitations have yet, spurred the search for a rather more elegant and economically viable strategy.

Another prevailing approach is to sensitize ZnO nanorods with semiconductor quantum dots (QDs), an increasingly promising strategy that offers a cost-effective and tunable means of red-shifting light absorption through the quantum confinement effect via dot-size adjustments [22, 23]. Of the many alternatives, PbS QDs stand out owing to their narrow bandgap (~0.41 eV for particles with ~18 nm in diameter, at room temperature), adjustable via particle size, enabling broadband absorption that can extend well into the near-infrared (NIR) region [24, 25]. Even though PbS QD incorporation has been proven to enhance ZnO-based photodetector performance under broadband illumination [26, 27], as demonstrated in Li et al.'s work, where ZnO nanorods coated with a PbS QD shell via the successive ionic layer adsorption and reaction (SILAR) method enabled broadband photodetection spanning from 340 nm to 840 nm [28], there still remains substantial room for in-depth studies. In particular, further investigations are needed to understand the charge transfer dynamics and to clarify the individual roles of each constituent material, with the broader goal of understanding how this material combination could be synergistically integrated with other ZnO-based hybrid structures.

In this study, we report a strategy to enhance RGO/ZnO NRs-based photodetectors with PbS QDs, using a simple, low-cost spray-coating technique. As a result, derived calculations from UV-Vis results revealed that by spray-coated of PbS QDs (2 mg mL^{-1}) onto ZnO NRs surfaces, our ZnO-PbS material's optical bandgap reduces from 3.19 eV to 3.13 eV. Notably, photoresponse measurements at 395 nm, a wavelength at the edge of the visible spectrum where the RGO/ZnO NRs device is less effective, showed a dramatic increase in photocurrent for the PbS-decorated counterpart, achieving a significantly enhanced photocurrent of 292.06 μA compared to just 17.447 μA for the unmodified device. In addition

to exhibiting a greater photocurrent response, the newly modified device also demonstrated outstanding operational stability over multiple on/off illumination cycles, with consistent and repeatable signal profiles. This dynamic reliability, combined with the improved figures of merit, such as enhanced photoresponsivity, photoconductive gain, specific detectivity, and signal reproducibility, underscores the practical promise of the RGO/ZnO–PbS system in broadband photodetection applications. Ultimately, these positives outcomes not only validate the strategy but also provides the essential groundwork for targeted future optimizations to maximize device performance.

2. Experimental Details

2.1. Materials

In this research, the following chemicals were used as received without any further purification: Graphene oxide nanoflakes (GO, 99%), zinc oxide nanoparticles (ZnO NPs, 99%, as a 40 wt% dispersion in ethanol), zinc nitrate hexahydrate ($(Zn(NO_3)_2.6H_2O$, 99%), hexamethylenetetramine (HMTA, $(CH_2)_6N_4$), 99%), lead sulfide quantum dots (PbS QDs, 99%), hydrazine hydrate solution (NH_2NH_2, 99.99%), and toluene (C_7H_8, 99.8%), were purchased from Sigma-Aldrich, while acetone ($(CH_3)_2CO$, 99.99%) and ethanol (C_2H_5OH, 99.99%) were purchased from Chemsol.

2.2. Synthesis of the RGO/ZnO and RGO/ZnO-PbS Heterostructures

ZnO nanorods were grown on glass substrates pre-coated with a reduced graphene oxide layer. Firstly, the RGO layer was prepared by reducing a spray-coated GO film with hydrazine hydrate as the reducing agent. Subsequently, the ZnO NRs were grown directly on the RGO surface via a one-step hydrothermal method. The detailed procedures for both the RGO preparation and ZnO NR growth are described in our previous publication [29]. To fabricate the sensitized samples, a solution of PbS QDs was prepared by diluting the stock solution in toluene to achieve a final concentration of 2 mg mL^{-1}. Then, this solution was deposited onto the surface of the as-prepared ZnO NRs/RGO substrates using a spray-coating method, after which they were dried at 40 °C for 10 minutes. This process yielded the final heterostructure, so-called RGO/ZnO-PbS, where PbS QDs decorate the ZnO NR surfaces.

2.3. Photodetector Fabrication

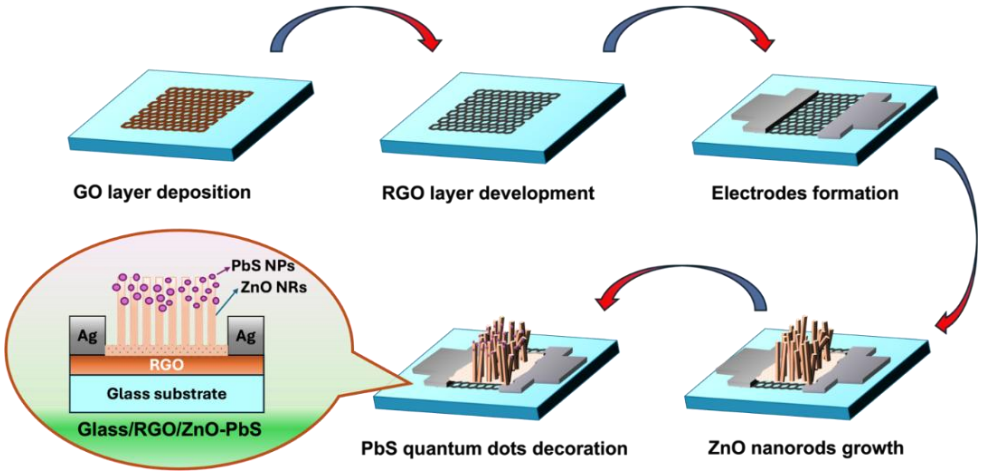

Figure 1. Schematic illustration of the fabrication process for the RGO/ZnO-PbS-based photodetector with Ag electrodes. The inset provides a cross-sectional view of our final device structure.

Planar photodetectors were fabricated using either RGO/ZnO or RGO/ZnO-PbS heterostructure as the active layer. A pair of silver (Ag) electrodes was deposited onto the surface of the conductive RGO layer via a sputtering method, with the support of a shadow mask, followed by the formation of photosensitive materials. The active area for each device was precisely defined as 1.4 mm × 2.0 mm. The main fabrication steps are summarized in Figure 1.

2.4. Characterization

The surface morphology and chemical composition of the materials were analyzed using a field-emission scanning electron microscope (FE-SEM) (JSM-6500F, JEOL Co. Ltd) and energy-dispersive X-ray (EDX) (Hitachi S-4800). The crystalline structure was investigated by X-ray diffraction (XRD) on a D8 Advance-Bruker system with CuKα radiation (λ = 1.54 Å). The optical properties of the pristine and PbS-decorated ZnO NRs were studied with a JASCO V670 UV-Vis spectrophotometer. Finally, the photoresponse performance of the devices was evaluated by current-voltage (*I-V*) and current-time (*I-t*) measurements on a Keithley 2400 source meter, using a 395 nm LED as the illumination source.

3. Results and Discussion

3.1. Structural and Optical Properties

To begin with, FESEM was utilized to examine the surface morphology of pristine ZnO NRs and PbS-decorated ZnO NRs, shown in Figures 2a and 2b, respectively. Both samples exhibit a dense layer of vertically aligned, hexagonal ZnO nanorods, each with an average diameter of approximately 100 nm. This well-defined morphology is consistent with the typical wurtzite crystal structural results [29], indicating a controlled synthesis process. Upon decoration with PbS quantum dots, it can be observed in Figure 2b that no significant changes in the overall ZnO nanostructure; instead, distinct PbS nanoparticles (highlighted in yellow) are distributed on the ZnO surfaces without aggregation or structural collapse. This moderate and homogeneous surface coverage suggests efficient interfacial contact between PbS and ZnO. The successful incorporation of PbS is coincidental with EDX analysis shown in Figure 2c, whereby characteristic signals of Pb and S are clearly detected alongside Zn and O. Elemental mapping also reveals an even spatial distribution of Pb and S, supporting the formation of a well-integrated hybrid system. In general, these findings prove the structural integrity and successful surface modification of ZnO NRs with PbS QDs, potentially promoting the formation of functional heterojunctions. The structural evaluation is further examined through XRD analysis in the following section.

Next, the crystal structure and phase purity of the synthesized materials were examined via X-ray diffraction. As presented in Figure 3a, the XRD pattern for ZnO NRs-PbS exhibits sharp and intense diffraction peaks that are well-indexed to the hexagonal wurtzite structure of ZnO, when compared with the synthesized ZnO NRs sample below, as well as file name JCPDS no. 36-1451 [30]. The pronounced intensity of (002) peaks in both synthesized samples suggest a preferential growth orientation along the *c*-axis of ZnO nanorod. Besides, the presence of heart-shaped marker indicating the (200) diffraction peak at $2\theta \approx 30.31°$ – corresponding to PbS, is well indexed with ICDD PDF no. 00-005-0592 [31], which also confirms the successful formation of ZnO-PbS heterostructure. Furthermore, a few weak peaks corresponding to zinc hydroxide ($Zn(OH)_2$) are observed, namely, at $2\theta \approx 28.65°$, which are likely associated with surface hydroxylation due to the sample's exposure to ambient conditions during measurement [32-34].

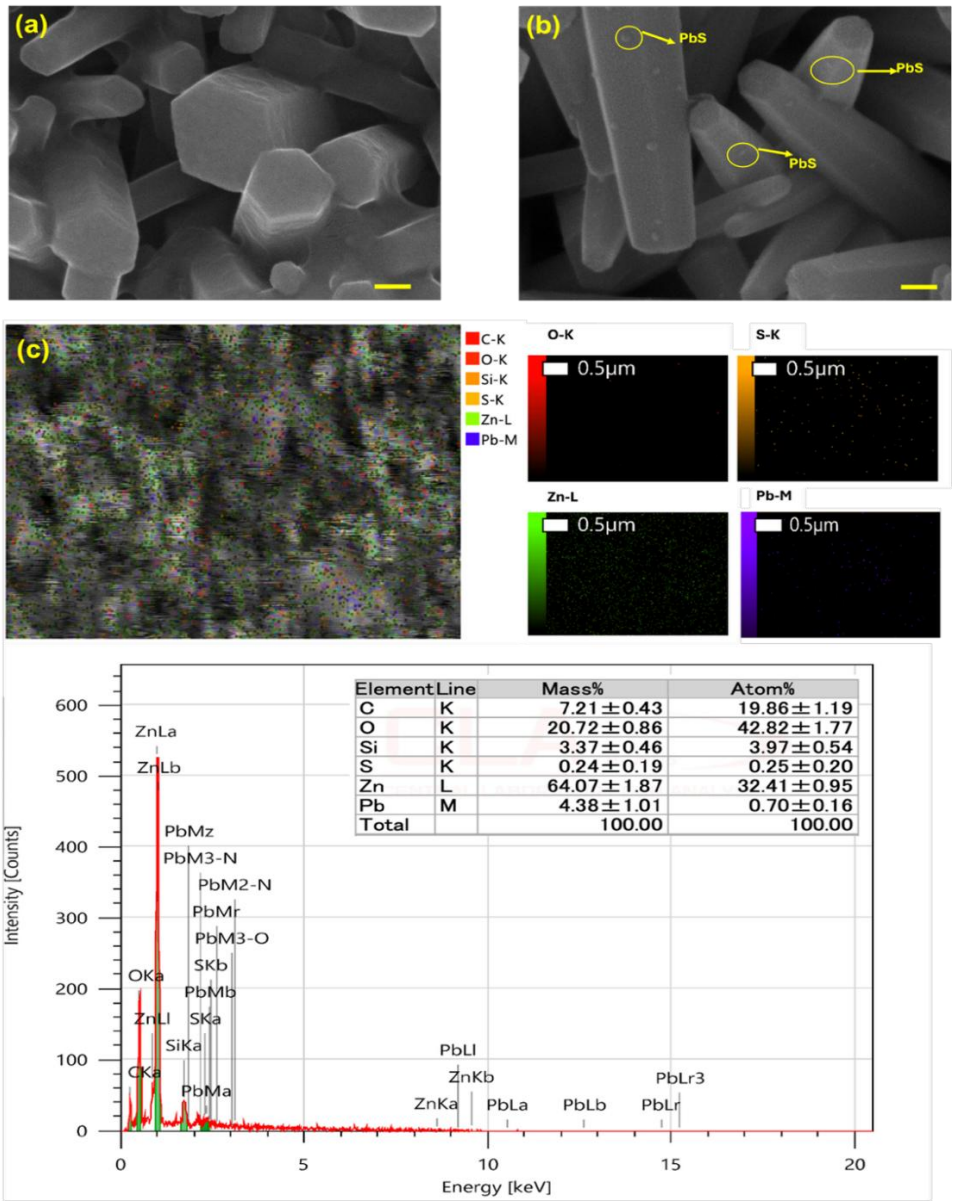

Figure 2. Morphological and compositional verification of the ZnO-PbS heterostructure. **(a-b)** Top-view FESEM images of ZnO nanorods before and after PbS QD decoration, respectively. PbS QDs are seen distributed across the ZnO surfaces without disrupting the nanorod morphology. **(c)** EDX elemental mapping and the corresponding spectrum of the final heterostructure, which confirm the successful incorporation and distribution of Zn, O, Pb, and S. The scale bars in **(a)** and **(b)** are 100 nm.

Consequently, to assess the impact of PbS sensitization on the light-harvesting capability of ZnO NRs, their optical properties were investigated using UV–Vis absorption spectroscopy. As can be observed from Figure 3b, the profound impact of PbS sensitization on the material's light-harvesting capability is clearly demonstrated in its optical properties. While the pristine ZnO NRs sample shows a sharp absorption edge limited to the UV region, consistent with reported studies on its wide bandgap, the ZnO-PbS composite, however, exhibits a strong, broadened absorption profile shifting towards longer wavelength regions. To quantify this effect, the optical bandgap (E_g) was determined using the

Tauc relation: $(\alpha hv)^{1/n} = A(hv - E_g)$ – where α is the absorption coefficient, hv is the photon energy, A is a constant, and $n = 1/2$ for the direct transition in ZnO [35]. Indeed, by extrapolating the linear portion extrapolating the linear portion of the $(\alpha hv)^2$ versus hv plot (Figure 3c), this analysis reveals a clear reduction of the pristine ZnO NRs optical bandgap from ca. 3.19 eV to 3.13 eV when decorated with PbS QDs. The observed bandgap reduction and corresponding absorption broadening can be attributed to a synergistic electronic interaction between PbS QDs and ZnO NRs, likely involving the formation of mid-gap states at the heterojunction interface [36-39]. Collectively, it is clear that PbS QDs could play an important role in enhancing the photo-absorption capability in the visible region of the ZnO host material, without affecting the hexagonal-like nanorod structure. Since the E_g value of RGO/ZnO–PbS is 3.13 eV (~396 nm), we then employed a visible 395 nm light source to measure the performance of our photodetectors.

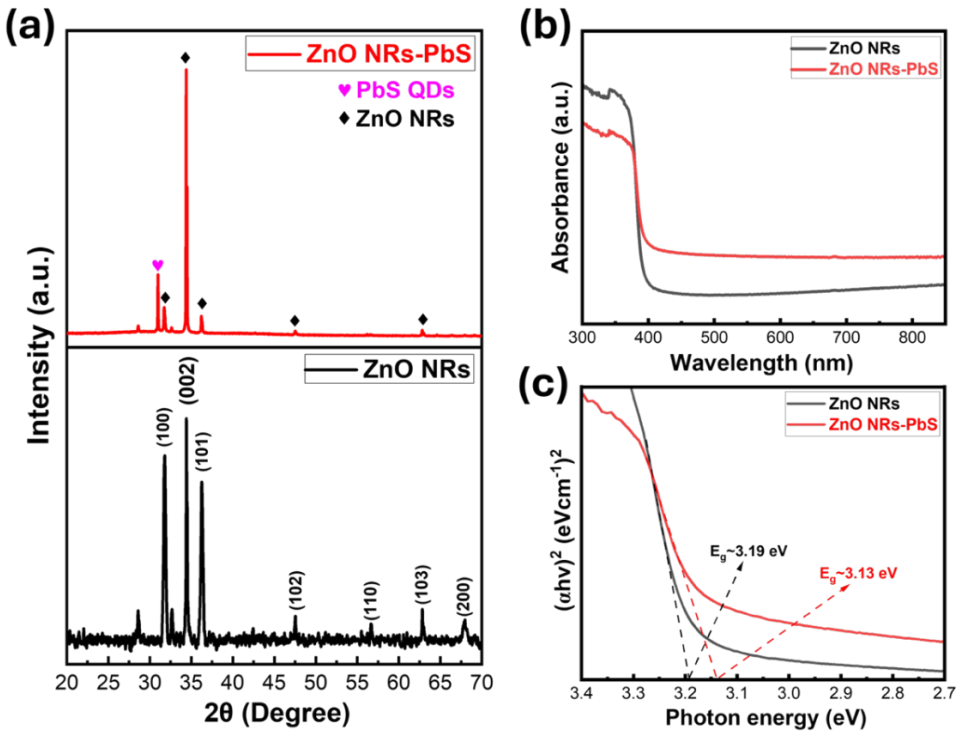

Figure 3. Structural and optical characterization of the active materials. **(a)** XRD patterns confirming the wurtzite crystalline structure of ZnO in both pristine and PbS-decorated samples. The additional peak (marked by heart symbol) in the latter is attributed to the successful integration of PbS QDs. **(b)** UV-Vis absorption spectra showing the significantly enhanced and broadened light absorption after PbS functionalization. **(c)** The corresponding Tauc plots, used to compare the optical bandgaps of RGO/ZnO and RGO/ZnO-PbS samples.

3.2. Photoelectronic Performance of Devices

Regarding to Figures 4a-c, the dramatic effect of the PbS QDs is immediately evident in the current-voltage (*I-V*) characteristics. At first, the RGO/ZnO device shows only a modest photoresponse, a weak photocurrent likely originating from absorption via band-tail states or surface defects within the ZnO nanostructure [5]. On the contrary, the introduction of PbS QDs leads to a noticeable amplification in photocurrent, increasing it by more than an order of magnitude under identical 395 nm illumination. This provides direct evidence that the PbS QDs act as highly effective sensitizers in improving the photonic signals of RGO/ZnO-PbS device. Furthermore, both devices, linear *I-V* curves confirm the

formation of excellent Ohmic contacts, ensuring efficient charge collection between the heterostructures materials with the electrodes.

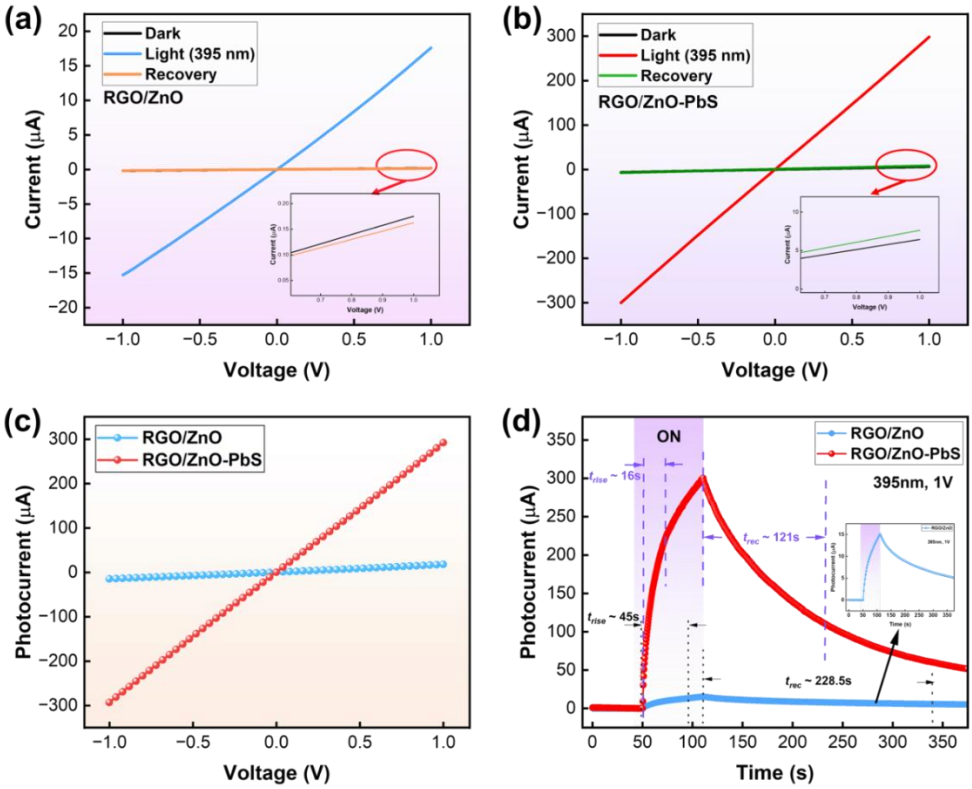

Figure 4. Photoresponse characteristics of the fabricated photodetectors. **(a-b)** Current-voltage (*I-V*) curves of the RGO/ZnO and RGO/ZnO-PbS devices, respectively. **(c)** Photocurrent comparison of the two devices. **(d)** Time-dependent photocurrent (I_{ph}-*t*) of the two devices. All measurements were conducted under a 1 V bias with 395 nm illumination for 50 s. The inset highlights the much weaker response of the pristine RGO/ZnO device for clarity.

Moving from static to dynamic behavior, the improvement of the sensitized device is further highlighted through time-dependent photocurrent (I_{ph}-*t*) measurements (Figure 4d). In this study, the photocurrent (I_{ph}) was calculated accordingly using the following formula:

$$I_{ph} = I_{light} - I_{dark}$$

where I_{dark} denotes the current measured in the absence of illumination, I_{light} refers to the current generated when the detector is exposed to light [40, 41]. To allow direct comparison, the corresponding *I–V* curves under identical lighting conditions were re-plotted in Figure 4c. The RGO/ZnO–PbS device exhibited a roughly 17x time higher photocurrent of 292.06 µA, compared to only 17.447 µA for the reference one without PbS. This dramatic increase highlights the substantial contribution of PbS QDs as active sensitizers.

In order to comprehensively evaluate the optoelectronic performance of RGO/ZnO-PbS NRs heterostructure, three key figures of merit were also taken into consideration, i.e. responsivity (*R*), photoconductive gain (*G*), and detectivity (*D**) [42-45]. We calculated these parameters using I–V data obtained under 395 nm illumination (800 µW). The calculations, which follow well-established methods from the literature, were based on the constant 1.4 × 2.0 mm^2 active area mentioned previously. The RGO/ZnO-PbS device demonstrated vastly superior performance compared to its pristine counterpart.

Its responsivity and gain reached 0.365 A W^{-1} and 1.146, respectively, whereas the RGO/ZnO device only managed modest values of 0.0187 A W^{-1} and 0.0587. Indeed, this remarkable photosensitivity was accompanied by a significant increase in dark current, rising from a very low 0.18 µA to 6.45 µA, indicated in the insets of Figure 4a-b. This is an anticipated trade-off, driven by two factors: first, the narrow bandgap of PbS promotes the creation of thermal carriers, and second, the added interface states provide new routes for dark current leakage [46]. However, the device's sensitivity is best captured through its specific detectivity, D^*, which accounts for both signal strength and noise [47]. Interestingly, D^*-value for the PbS-decorated device still improved to 3.82×10^{10} Jones – roughly three times higher than the pristine device's 1.30×10^{10} Jones – highlighting that the gain in signal generation far outweighs the moderate increase in noise. The key to this device's excellent performance lies in what the PbS quantum dots are doing. First, they broaden the device's absorption to include more of the light spectrum. Second, they create an internal gain by trapping holes, which keeps the electrons active for longer and boosts the signal [48, 49]. On top of that, the RGO/ZnO-PbS device was also much faster, as shown in Figure 4d, as its response and recovery times (16s/121s) were significantly better than the device without PbS (46s / 228.5s). These aforementioned results indicate the crucial role of PbS QDs in improving both charge collection and recombination efficiency [50, 51].

Finally, cyclic time-dependent photocurrent experiments were carried out to assess our RGO/ZnO-PbS photodetector's dynamic response and operational stability in ambient conditions. When exposed to 395 nm light, the device generated a significant photocurrent that consistently peaked at approximately 270 µA. The device shows excellent stability, as displayed in Figure 5, the peak current barely dropped even after many on/off cycles, which is crucial for long-term reliability. However, there's a major drawback: the device's temporal response to light cessation. Since deep-level trap states are frequently found in ZnO-based materials, the decay process is noticeably slow, suggesting a slow carrier recombination mechanism that exhibits a strong pronounced persistent photoconductivity (PPC) impact, this commonsense phenomenon has been reported in numerous works, such as from K. Kandpal et al., and Haldorai et al., [52, 53]. Despite the device's remarkable sensitivity and stability, its use for high-speed photodetection is ultimately limited by its sluggish decay, which also leads to a partial recovery to the starting dark current within the 50-second off-period.

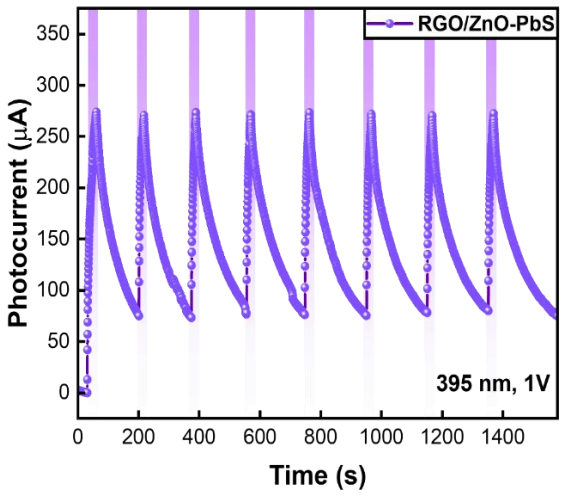

Figure 5. Photoresponse and stability of the RGO/ZnO-PbS photodetector. Time-dependent photocurrent (I_{ph}-t) curve of the device measured at a 1 V bias under periodic illumination from a 395 nm light source. The light purple shaded regions indicate the periods when the light was on (~20 s), followed by dark periods (~50 s) in white. The consistent peak photocurrent across multiple cycles highlights the excellent operational stability and reproducibility of the device.

3.3. Mechanism of PbS-decorated Photodetection

Given the clear synergistic enhancement observed in the previous results, herein, Figure 6 illustrates the proposed working principle of our RGO/ZnO-PbS photodetector, depending on how different materials in the device interact under dark and illuminated conditions. In dark conditions (Figure 6a), the device is in a stable, equilibrium state. Because the materials have different energy levels, their energy bands realign at their interfaces, creating internal built-in electric fields (ε_{int}) [54]. At the RGO/ZnO interface, a *p–n* junction forms, resulting in downward band bending on the ZnO side and the emergence of an internal electric field directed from ZnO toward RGO [55, 56]. Concurrently, oxygen molecules from the surrounding air being adsorbed to the semiconductor surfaces and trap free electrons ($O_2 + e^- \rightarrow O_2^-$). This process forms a wide depletion region on the surface of ZnO NRs and PbS QDs, suppresses the flow of charge carriers and results in a low dark current [57, 58].

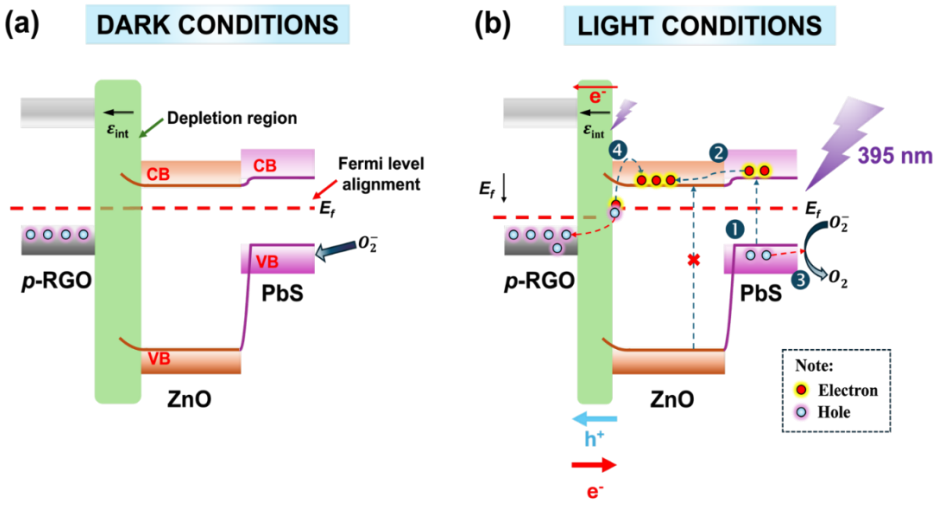

Figure 6**.** Proposed photodetection mechanism in the RGO/ZnO-PbS heterostructure. The schematic shows the energy band alignment and charge carrier dynamics **(a)** in the dark (thermal equilibrium) and **(b)** under 395 nm light illumination. The Fermi level (E_f), conduction band (CB), valence band (VB), and intrinsic electrical field (ε_{int}) are indicated.

Under 395 nm illumination (Figure 6b), the device's photoresponse is initiated solely by the PbS QDs, which absorb the photons while the ZnO mostly remains inert. This absorption generates electron-hole pairs in PbS QDs (*route (1)*), after which the ZnO then acts as an electron transport layer, efficiently channeling these electrons away from the PbS and toward the RGO interface (*route (2)*). This efficient two-step charge separation at the ZnO/PbS junction is the foundation of the device's enhanced performance. Meanwhile, the remaining holes in the PbS migrate to the surface, where they combine with trapped oxygen ions and release them as oxygen gas ($h^+ + O_2^- \rightarrow O_2$) (*route (3)*). This efficient separation of charge creates the device's dominant sensing mechanism: the photogating effect [59, 60]. The long-lived holes trapped within the PbS QDs form a stable layer of positive charge. This layer functions as a "photogate," applying a powerful electric field that modulates the conductivity of the RGO channel below. Since the RGO channel is mostly considered as *p*-type, this positive gate attracts an influx of additional holes from the source electrode to maintain charge neutrality, significantly increasing the channel's overall conductivity [61]. This surge in mobile carrier concentration dramatically increases the conductivity of the RGO layer. Furthermore, the intrinsic field at the RGO/ZnO junction facilitates interfacial excitation: electrons near this region, particularly from shallow

traps or sub-bandgap states in ZnO, are promoted into the CB, while holes are swept into the RGO layer via *route (4)* [62, 63]. The rising hole density in RGO enhances its photoconductivity by shifting its quasi-Fermi level. Under external applied bias, this RGO layer provides a rapid transport path to the electrodes, resulting in efficient carrier collection and an initial photocurrent spike. However, prolonged exposure enables a counter-effect: thermally excited electrons from the ZnO migrate back to the RGO, where they recombine with holes. Also, it is worth mentioning that not all the excited electrons take the forward path. Some can fall back to lower energy levels inside the QD or return from the ZnO conduction band to the QD, as stated in Sambur et al.'s work [64]. For these reasons, the hole population would deplete and ultimately causes the photocurrent to level off, or saturate. When the light is turned off, the electrons and holes quickly recombine, especially thanks to the efficient RGO pathway. The full recovery of our device is pertinently controlled by a slower process: oxygen molecules from the air gradually re-adsorb onto the surface, restoring the depletion region and returning the device to its original high-resistance state [65]. While the dominant direction of Fermi level modulation in our device has not been conclusively determined, the existence of a photogating effect remains a plausible and complementary contributor to the observed photoresponse [66].

4. Conclusion

In summary, we have successfully fabricated a low-cost photo- detector based on a RGO/ZnO-PbS hybrid structure through a simple solution route, which exhibits a fast and stable response to 395-nm light source. The PbS QD decoration, at first, reconfigured the photon intake of our device by narrowing the overall optical bandgap to 3.13 eV, while keeping the surface morphology of pristine ZnO NRs intact. Furthermore, we compared its performance to a pristine RGO/ZnO device, in order to highlight the critical role of the quantum dots. The RGO/ZnO-PbS device showed significant enhancements, achieving a response/recovery time of 16s / 121s and a peak photocurrent of 292.06 μA (at 800 μW cm^{-2}). Combines with improved key performance metrics, i.e., a responsivity of 0.365 A W^{-1}, a photoconductive gain of 1.15, and a detectivity of 3.82×10^{10} Jones, the device also displayed a stable photocurrent over several on/off cycles, confirming its reliability and repeatability. Therefore, we believe that these results demonstrate the RGO/ZnO-PbS hybrid is a promising platform for developing low-cost, high-performance spectral response of ZnO-based photodetectors towards visible regime for future applications.

CRediT Authorship Contribution Statement

G. V. Le and N. Q. K. Le: Investigation, Writing – original draft, Data curation, Visualization, Formal analysis, Conceptualization. T. P. Tran and V. A. T. Vo: Investigation. K. Q. Luu: Conceptualization. H. T. M. Hoa, K. N. Pham and C. K. Tran: Formal analysis, Data curation. P. P. H. La and L. T. Duy: Conceptualization, Visualization, Writing – review & editing, Data curation. V. Q. Dang: Resources, Conceptualization, Supervision, Writing – review & editing.

Acknowledgments

This research is funded by Vietnam National Foundation for Science and Technology Development (NAFOSTED) under grant number 103.03-2021.59.

References

[1] Y. Xiong, J. Chen, Y. Lu, and F. Xu, Heterostructures: Broadband Optical-Fiber-Compatible Photodetector Based on a Graphene-MoS_2-WS_2 Heterostructure with a Synergetic Photogenerating Mechanism (Adv. Electron. Mater. 1/2019), Advanced Electronic Materials, Vol. 5, No. 1, 2019, https://doi.org/10.1002/aelm.201970005.

[2] A. M. Afzal, G. Dastgeer, M. Z. Iqbal, P. Gautam, M. M. Faisal, High-Performance p-BP/n-$PdSe_2$ Near-Infrared Photodiodes with a Fast and Gate-Tunable Photoresponse, ACS Applied Materials & Interfaces, Vol. 12, No. 17, 2020, pp. 19625–19634, https://doi.org/10.1021/acsami.9b22898.

[3] Z. T. Li et al., Investigation of Light-Extraction Mechanisms of Multiscale Patterned Arrays With Rough Morphology for GaN-Based Thin-Film LEDs, IEEE Access, Vol. 7, 2019, pp. 73890-73898, https://doi.org/10.1109/access.2019.2921058.

[4] Y. Lee et al., Effectual Interface and Defect Engineering for Auger Recombination Suppression in Bright InP/ZnSeS/ZnS Quantum Dots, ACS Applied Materials & Interfaces, Vol. 14, No. 10, 2022, pp. 12479-12487, https://doi.org/10.1021/acsami.1c20088.

[5] D. N. Giang et al., A Visible-Light Photodetector Based on Heterojunctions between CuO Nanoparticles and ZnO Nanorods, Beilstein Journal of Nanotechnology, Vol. 14, 2023, pp. 1018-1027, https://doi.org/10.3762/bjnano.14.84.

[6] L. Huang, S. Zaman, X. Tian, Z. Wang, W. Fang, B. Y. Xia, Advanced Platinum-Based Oxygen Reduction Electrocatalysts for Fuel Cells, Accounts of Chemical Research, Vol. 54, No. 2, 2021, pp. 311-322, https://doi.org/10.1021/acs.accounts.0c00488.

[7] W. Khan et al., Efficient and Continuous Microwave Photoconversion in Hybrid Cavity-Semiconductor Nanowire Double Quantum Dot Diodes, Nature Communications, Vol. 12, No. 1, 2021, pp. 5130, https://doi.org/10.1038/s41467-021-25446-1.

[8] M. Ding, Z. Guo, X. Chen, X. Ma, L. Zhou, Surface/Interface Engineering for Constructing Advanced Nanostructured Photodetectors with Improved Performance: A Brief Review, Nanomaterials, Vol. 10, No. 2, 2020, pp. 362, https://doi.org/10.3390/nano10020362.

[9] H. Dong et al., Innovative All-Silicon Based a-SiNx:O/c-Si Heterostructure Solar-Blind Photodetector with Both High Responsivity and Fast Response Speed, APL Photonics, Vol. 7, No. 2, 2022, pp. 026102, https://doi.org/10.1063/5.0071602.

[10] Y. Xia et al., Confined Formation of Ultrathin ZnO Nanorods/Reduced Graphene Oxide Mesoporous Nanocomposites for High-Performance Room-Temperature NO_2 Sensors, ACS Applied Materials & Interfaces, Vol. 8, No. 51, 2016, pp. 35454-35463, https://doi.org/10.1021/acsami.6b12501.

[11] S. Prabhu et al., Synthesis, Structural and Optical Properties of ZnO Spindle/Reduced Graphene Oxide Composites with Enhanced Photocatalytic Activity under Visible Light Irradiation, Optical Materials, Vol. 79, 2018, pp. 186-195, https://doi.org/10.1016/j.optmat.2018.02.061.

[12] M. B. Akturk, M. Toufani, A. Tufani, E. Erdem, ZnO and Reduced Graphene Oxide Electrodes for All-in-One Supercapacitor Devices, Nanoscale, Vol. 14, No. 8, 2022, pp. 3269-3278, https://doi.org/10.1039/D2NR00018K.

[13] D. Panda, T. Y. Tseng, One-Dimensional ZnO Nanostructures: Fabrication, Optoelectronic Properties, and Device Applications, Journal of Materials Science, Vol. 48, No. 20, 2013, pp. 6849-6877, https://doi.org/10.1007/s10853-013-7541-0.

[14] W. Ouyang, J. Chen, Z. Shi, X. Fang, Self-Powered UV Photodetectors Based on ZnO Nanomaterials, Applied Physics Reviews, Vol. 8, No. 3, 2021, pp. 031315, https://doi.org/10.1063/5.0058482.

[15] K. Liu, M. Sakurai, M. Aono, ZnO-Based Ultraviolet Photodetectors, Sensors, Vol. 10, No. 9, 2010, pp. 8604-8634, https://doi.org/10.3390/s100908604.

[16] Q. Zhu, C. Xie, H. Li, C. Yang, S. Zhang, and D. Zeng, Selectively Enhanced UV and NIR Photoluminescence from a Degenerate ZnO Nanorod Array Film, Journal of Materials Chemistry C, Vol. 2, No. 23, 2014, pp. 4566, https://doi.org/10.1039/c4tc00011k.

[17] Z. Li et al., Electro-optic Effect of ZnO Microcavity and Active Dynamic Lasing Mode Modulation, Advanced Optical Materials, Vol. 10, No. 19, 2022, pp. 2201080, https://doi.org/10.1002/adom.202201080.

[18] D. D. Thongam, H. Chaturvedi, Heterostructure Charge Transfer Dynamics on Self-Assembled ZnO on Electronically Different Single-Walled Carbon Nanotubes, Chemosphere, Vol. 323, 2023, pp. 138239, https://doi.org/10.1016/j.chemosphere.2023.138239.

[19] S. J. Young, Y.L. Chu, Platinum Nanoparticle-Decorated ZnO Nanorods Improved the Performance of Methanol Gas Sensor, Journal of The Electrochemical Society, Vol. 167, No. 14, 2020, pp. 147508, https://doi.org/10.1149/1945-7111/abc4be.

[20] Y. L. Chu et al., Characteristics of Gas Sensors Based on Co-Doped ZnO Nanorod Arrays, Journal of the Electrochemical Society, Vol. 167, No. 11, 2020, pp. 117503, https://doi.org/10.1149/1945-7111/aba00d.

[21] T. Zhang et al., Multi-Component ZnO Alloys: Bandgap Engineering, Hetero-Structures, and Optoelectronic Devices, Materials Science and Engineering: R: Reports, Vol. 147, 2022, pp. 100661, https://doi.org/10.1016/j.mser.2021.100661.

[22] Y. A. Douri, M. M. Khan, J. R. Jennings, Synthesis and Optical Properties of II–VI Semiconductor Quantum Dots: A Review, Journal of Materials Science: Materials in Electronics, Vol. 34, No. 11, 2023, pp. 993, https://doi.org/10.1007/s10854-023-10435-5.

[23] Electro-Materials Research Laboratory, Centre for Nanoscience and Technology, Pondicherry University, Puducherry-605014, India et al., Recent Developments in Metal Chalcogenides Based Quantum Dot Sensitized Solar Cells, ES Energy & Environment, 2022, https://doi.org/10.30919/esee8c754.

[24] S. A. McDonald et al., Solution-Processed PbS Quantum Dot Infrared Photodetectors and Photovoltaics, Nature Materials, Vol. 4, No. 2, 2005, pp. 138-142, https://doi.org/10.1038/nmat1299.

[25] Z. Sun, Z. Liu, J. Li, G. Tai, S. Lau, F. Yan, Infrared Photodetectors Based on CVD-Grown Graphene and PbS Quantum Dots with Ultrahigh Responsivity, Advanced Materials, Vol. 24, No. 43, 2012, pp. 5878-5883, https://doi.org/10.1002/adma.201202220.

[26] X. Wang et al., Amorphous ZnO/PbS Quantum Dots Heterojunction for Efficient Responsivity Broadband Photodetectors, ACS Applied Materials & Interfaces, Vol. 12, No. 7, 2020, pp. 8403-8410, https://doi.org/10.1021/acsami.9b19486.

[27] J. M. Szarko et al., Photovoltaic Function and Exciton/Charge Transfer Dynamics in a Highly Efficient Semiconducting Copolymer, Advanced Functional Materials, Vol. 24, No. 1, 2014, pp. 10-26, https://doi.org/10.1002/adfm.201301820.

[28] H. Li et al., An Interfacial Defect-Controlled ZnO/PbS QDs/ZnS Heterostructure Based Broadband Photodetector, RSC Advances, Vol. 6, No. 78, 2016, pp. 74575-74581, https://doi.org/10.1039/C6RA14574D.

[29] L. N. Q. Khoi et al., Improving ZnO-Based Photodetectors via Mn Doping and RGO Integration for Visible Light Sensitivity, Sensors and Actuators A: Physical, Vol. 389, 2025, pp. 116576, https://doi.org/10.1016/j.sna.2025.116576.

[30] V. V. Kutwade, K. P. Gattu, A. S. Dive, M. E. Sonawane, D. A. Tonpe, R. Sharma, Enhanced Photosensing by Mg-Doped ZnO Hexagonal Rods via a Feasible Chemical Route, Journal of Materials Science: Materials in Electronics, Vol. 32, No. 5, 2021, pp. 6475-6486, https://doi.org/10.1007/s10854-021-05364-0.

[31] L. Yuan et al., Air-Stable PbS Quantum Dots Synthesized with Slow Reaction Kinetics via a $PbBr_2$ Precursor, RSC Advances, Vol. 5, No. 84, 2015, pp. 68579-68586, https://doi.org/10.1039/C5RA13499D.

[32] E. V. Polyakov, M. A. Maksimova, Y. V. Kuznetsova, L. Yu. Buldakova, Colloidal-chemical Mechanism of Zn(OH)2-ZnO Layer Formation at the Glass - Ammonia Solution - Zn(II) Interface, Nanosystems: Physics, Chemistry, Mathematics, Vol. 14, No. 2, 2023, pp. 231-241, https://doi.org/10.17586/2220-8054-2023-14-2-231-241.

[33] M. Faheem, H. M. Siddiqi, A. Habib, M. Shahid, A. Afzal, ZnO/Zn(OH)2 Nanoparticles and Self-Cleaning Coatings for the Photocatalytic Degradation of Organic Pollutants, Frontiers in Environmental Science, Vol. 10, 2022, pp. 965925, https://doi.org/10.3389/fenvs.2022.965925.

[34] D. A. Giannakoudakis, J. A. A. Orozco, T. J. Bandosz, Key Role of Terminal Hydroxyl Groups and Visible Light in the Reactive Adsorption/Catalytic Conversion of Mustard Gas Surrogate on Zinc (Hydr)Oxides, Applied Catalysis B: Environment and Energy, Vol. 174-175, 2015, pp. 96-104, https://doi.org/10.1016/j.apcatb.2015.02.028.

[35] A. S. Trevizo, P. A. Madrid, P. P. Ruiz, W. A. Flores, M. M. Yoshida, Optical Band Gap Estimation of ZnO Nanorods, Materials Research, Vol. 19, No. suppl 1, 2016, pp. 33-38, https://doi.org/10.1590/1980-5373-mr-2015-0612.

[36] W. Gong, P. Wang, D. Dai, Z. Liu, L. Zheng, Y. Zhang, Infrared Colloidal Quantum Dots for Photoelectric Conversion Devices, Journal of Materials Chemistry C, Vol. 9, No. 9, 2021, pp. 2994-3025, https://doi.org/10.1039/D0TC05902A.

[37] Y. Liang, T. Novet, J. E. Thorne, B. A. Parkinson, Photosensitization of ZnO Single Crystal Electrodes with PbS Quantum Dots: Photosensitization of ZnO Single Crystal Electrodes with PbS QDs, Physica Status Solidi (a), Vol. 211, No. 9, 2014, pp. 1954-1959, https://doi.org/10.1002/pssa.201330602.

[38] D. Yan, M. Liu, Z. Li, B. Hou, Colloidal Quantum Dots and Metal Halide Perovskite Hybridization for Solar Cell Stability and Performance Enhancement, Journal of Materials Chemistry A, Vol. 9, No. 28, 2021, pp. 15522-15541, https://doi.org/10.1039/D1TA02214H.

[39] P. H. Chen et al., Enhanced Photocurrent and Responsivity of PbS Quantum Dot/ZnO Nanoparticle Films with Amine Passivation, Applied Surface Science Advances, Vol. 26, 2025, pp. 100705, https://doi.org/10.1016/j.apsadv.2025.100705.

[40] X. Han, W. Du, R. Yu, C. Pan, Z. L. Wang, Piezo-Phototronic Enhanced UV Sensing Based on a Nanowire Photodetector Array, Advanced Materials, Vol. 27, No. 48, 2015, pp. 7963-7969, https://doi.org/10.1002/adma.201502579.

[41] A. B. Kaul, Triple-cation Perovskite Solar Cells with An Inorganic Two-Dimensional Tungsten Diselenide Hole Transport Layer for Moisture Stability, in Energy Harvesting and Storage: Materials, Devices, and Applications XV, P. Bermel, N. C. Das, and Z. Omair, Eds., Orlando, United States: SPIE, May 2025, pp. 3. https://doi.org/10.1117/12.3054132.

[42] G. Hasnain, B. F. Levine, S. Gunapala, N. Chand, Large Photoconductive Gain in Quantum Well Infrared Photodetectors, Applied Physics Letters, Vol. 57, No. 6, 1990, pp. 608-610, https://doi.org/10.1063/1.103612.

[43] G. Luo et al., Enhanced Performance of ZnO Nanorod Array/CuSCN Ultraviolet Photodetectors with Functionalized Graphene Layers, RSC Advances, Vol. 11, No. 13, 2021, pp. 7682-7692, https://doi.org/10.1039/D0RA10420E.

[44] P. Vashishtha, P. Goswami, P. Prajapat, A. Kumar Gangwar, P. Singh, G. Gupta, Highly Efficient, Self-Powered, and Air-Stable Broadband Photodetector Based on SnSe Thin Film, Materials Science and Engineering: B, Vol. 297, 2023, pp. 116808, https://doi.org/10.1016/j.mseb.2023.116808.

[45] S. Huang et al., Broadband-Spectral-Responsivity of Black Silicon Photodetector with High Gain and Sub-Bandgap Sensitivity by Titanium Hyperdoping, Optics & Laser Technology, Vol. 171, 2024, pp. 110399, https://doi.org/10.1016/j.optlastec.2023.110399.

[46] B. K. Jung et al., Suppressing the Dark Current in Quantum Dot Infrared Photodetectors by Controlling Carrier Statistics, Advanced Optical Materials, Vol. 10, No. 2, 2022, pp. 2101611, https://doi.org/10.1002/adom.202101611.

[47] P. Vashishtha et al., CVD-Grown Monolayer MoS_2 and GaN Thin Film Heterostructure for a Self-Powered and Bidirectional Photodetector with an Extended Active Spectrum, ACS Applied Materials & Interfaces, Vol. 16, No. 24, 2024, pp. 31294–31303, https://doi.org/10.1021/acsami.4c03902.

[48] K. Chauhan, A. K. Pandey, M. Bhattacharjee, Quantum Dot-Based Flexible Photodetectors: A Review, ACS Applied Electronic Materials, Vol. 7, No. 9, 2025, pp. 3632-3649, https://doi.org/10.1021/acsaelm.5c00304.

[49] J. Miao, F. Zhang, Recent Progress on Photomultiplication Type Organic Photodetectors, Laser & Photonics Reviews, Vol. 13, No. 2, 2019, pp. 1800204, https://doi.org/10.1002/lpor.201800204.

[50] C. Liu, K. Wang, P. Du, E. Wang, X. Gong, A. J. Heeger, Ultrasensitive Solution-Processed Broad-Band Photodetectors Using CH_3 NH_3 PbI_3 Perovskite Hybrids and PbS Quantum Dots as Light Harvesters, Nanoscale, Vol. 7, No. 39, 2015, pp. 16460-16469, https://doi.org/10.1039/C5NR04575D.

[51] U. Bothra, M. A. Siguan, Y. Vaynzof, D. Kabra, Impact of Ligands on the Performance of PbS Quantum Dot Visible–Near-Infrared Photodetectors, Advanced Optical Materials, Vol. 11, No. 1, 2023, pp. 2201897, https://doi.org/10.1002/adom.202201897.

[52] Y. Haldorai, W. Voit, J. J. Shim, Nano ZnO@reduced Graphene Oxide Composite for High Performance Supercapacitor: Green Synthesis in Supercritical Fluid, Electrochimica Acta, Vol. 120, 2014, pp. 65-72, https://doi.org/10.1016/j.electacta.2013.12.063.

[53] K. Kandpa, N. Gupta, Perspective of Zinc Oxide Based Thin Film Transistors: A Comprehensive Review, Microelectronics International, Vol. 35, No. 1, 2018, pp. 52-63, https://doi.org/10.1108/MI-10-2016-0066.

[54] Z. Yang, M. Wang, X. Song, G. Yan, Y. Ding, J. Bai, High-Performance ZnO/Ag Nanowire/ZnO Composite Film UV Photodetectors with Large Area and Low Operating Voltage, Journal of Materials Chemistry C, Vol. 2, No. 21, 2014, pp. 4312-4319, https://doi.org/10.1039/C4TC00394B.

[55] A. R. McNeill, A. R. Hyndman, R. J. Reeves, A. J. Downard, M. W. Allen, Tuning the Band Bending and Controlling the Surface Reactivity at Polar and Nonpolar Surfaces of ZnO through Phosphonic Acid Binding, ACS Applied Materials & Interfaces, Vol. 8, No. 45, 2016, pp. 31392-31402, https://doi.org/10.1021/acsami.6b10309.

[56] K. Zhao et al., Self-Powered Photoelectrochemical Biosensor Based on CdS/RGO/ZnO Nanowire Array Heterostructure, Small, Vol. 12, No. 2, 2016, pp. 245-251, https://doi.org/10.1002/smll.201502042.

[57] H. Liu, Q. Dong, R. Lopez, The Effect of Light Intensity, Temperature, and Oxygen Pressure on the Photo-Oxidation Rate of Bare PbS Quantum Dots, Nanomaterials, Vol. 8, No. 5, 2018, pp. 341, https://doi.org/10.3390/nano8050341.

[58] H. T. Dastjerdi, D. Prochowicz, P. Yadav, M. M. Tavakoli, Tuning Areal Density and Surface Passivation of ZnO Nanowire Array Enable Efficient PbS QDs Solar Cells with Enhanced Current Density, Advanced Materials Interfaces, Vol. 7, No. 1, 2020, pp. 1901551, https://doi.org/10.1002/admi.201901551.

[59] J. Ge et al., Self-Aligned Heterojunction Gate Carbon Nanotube Phototransistors for Highly Sensitive Infrared Detection, Advanced Electronic Materials, Vol. 11, No. 11, 2025, pp. 2400966, https://doi.org/10.1002/aelm.202400966.

[60] X. Xia et al., Ultralow Dark Current and High-Detectivity Infrared Phototransistors Enabled by Small-Diameter Semiconducting Carbon Nanotubes, Advanced Functional Materials, Vol. 34, No. 48, 2024, pp. 2408368, https://doi.org/10.1002/adfm.202408368.

[61] S. Chakraborty, A. N. Resmi, P. R. Devi, K. B. Jinesh, P-Channel Thin Film Transistors Using Reduced Graphene Oxide, Nanotechnology, Vol. 28, No. 15, 2017, pp. 155201, https://doi.org/10.1088/1361-6528/aa628d.

[62] H. Liu et al., Fast and Enhanced Broadband Photoresponse of a ZnO Nanowire Array/Reduced Graphene Oxide Film Hybrid Photodetector from the Visible to the Near-Infrared Range, ACS Applied Materials & Interfaces, Vol. 7, No. 12, 2015, pp. 6645-6651, https://doi.org/10.1021/am509084r.

[63] T. N. Reddy, J. Manna, R. K. Rana, Polyamine-Mediated Interfacial Assembly of rGO-ZnO Nanostructures: A Bio-Inspired Approach and Enhanced Photocatalytic Properties, ACS Applied Materials & Interfaces, Vol. 7, No. 35, 2015, pp. 19684-19690, https://doi.org/10.1021/acsami.5b04820.

[64] J. B. Sambur, T. Novet, B. A. Parkinson, Multiple Exciton Collection in a Sensitized Photovoltaic System, Science, Vol. 330, No. 6000, 2010, pp. 63-66, https://doi.org/10.1126/science.1191462.

[65] M. Kim, J. Beak, S. Kim, W. S. Hwang, B. J. Cho, M. Shin, Impact of Oxygen Deficiency and Shallow Hole-Traps on High-Responsivity ZnO-Based UV Photodetectors, Sensors and Actuators A: Physical, Vol. 369, 2024, pp. 115160, https://doi.org/10.1016/j.sna.2024.115160.

[66] P. Abid, P. Sehrawat, S. S. Islam, P. Mishra, S. Ahmad, Reduced Graphene Oxide (rGO) Based Wideband Optical Sensor and the Role of Temperature, Defect States and Quantum Efficiency, Scientific Reports, Vol. 8, No. 1, 2018, pp. 3537, https://doi.org/10.1038/s41598-018-21686-2.